Journal on Electronic and Automation Engineering

Vol: 4(1), March 2025

REST Publisher; ISSN: 2583-6951 (Online)

Website: https://restpublisher.com/journals/jeae/

DOI: https://doi.org/10.46632/jeae/4/1/8

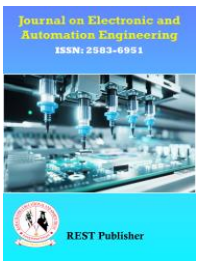

A Novel Wind Energy Integration and MPPT Algorithm based Multi-Input Multi-Output DC/DC Converter

[*]P. Rama Mohan, A. Mohan Babu, P. Shashanka,
K. Kamalakar, P. Lakshmi Narasimha Var Prasad, S. Yousuf Ali

Annamacharya Institute of Technology & Sciences (Autonomous) Kadapa, Andhra Pradesh, India.
[*] Corresponding Author E-mail: rammohan.kadapa@gmail.com

Abstract: *This study presents the development of a high-efficiency multi-input multi-output (MIMO) DC/DC converter integrated with wind energy and a wind maximum power point tracking (MPPT) algorithm for renewable energy applications. In renewable energy systems, particularly those utilizing wind power, multiple output voltages are often required to power various loads, while optimizing energy conversion efficiency. The proposed MIMO DC/DC converter accommodates multiple input sources, including wind turbines, while achieving high step-up voltage conversion to provide stable output voltages for different applications. The converter utilizes a coupled inductor with a low turn ratio to enhance voltage gain, while the MPPT algorithm ensures maximum power extraction from the wind turbine by continuously adjusting to the changing wind conditions. The converter employs soft-switching techniques, including voltage clamping and zero-voltage switching (ZVS), to improve efficiency by reducing switching losses. Additionally, an auxiliary inductor regulates the voltage of the auxiliary output, enabling effective energy management across multiple outputs. Experimental results validate the high efficiency and performance of the proposed converter, demonstrating its suitability for wind power generation and other renewable energy systems requiring multi-output configurations.*

1. INTRODUCTION

Renewable energy systems, especially those that integrate wind power, have gained considerable attention in recent years as a means to address the growing energy demands while mitigating the environmental impact of conventional energy sources. Wind energy, in particular, offers several advantages, such as a renewable and widely available resource. However, to fully utilize the potential of wind turbines, efficient power conversion systems and advanced control techniques are crucial for optimizing energy extraction and distribution. Among the key components in such systems are power converters, which manage energy flow from the wind turbine to the electrical grid or various loads. Traditional power converters, however, face limitations when handling multiple inputs and outputs, especially when varying wind conditions demand dynamic responses in power generation and distribution. This has led to the development of advanced converters, such as Multi-Input Multi-Output (MIMO) DC/DC converters, to improve the efficiency and performance of renewable energy systems.

Renewable Energy and Wind Power Systems: The growing interest in renewable energy systems is driven by the need for sustainable alternatives to fossil fuels. Wind energy, in particular, has become one of the most promising sources of renewable power due to its cost-effectiveness and environmentally friendly nature. Wind turbines convert kinetic energy from the wind into electrical energy, which can then be used to power homes, industries, and the electrical grid. However, the energy produced by wind turbines is highly variable, as wind speeds fluctuate with time and location. This variability necessitates the use of sophisticated control techniques to ensure that the generated power is efficiently harvested, converted, and distributed. A critical aspect of wind energy systems is the power conversion process. The output from wind turbines is typically in the form of alternating current (AC), which often needs to be converted to direct current (DC) or to specific voltage levels suitable for various applications. Additionally, as wind turbines operate under different environmental conditions, the amount of power generated can vary significantly. This variability poses challenges in maintaining stable power output that meets the demands of connected loads.

Challenges in Wind Power Conversion: Wind power conversion systems face several challenges, the most significant of which are related to energy efficiency and adaptability to changing wind conditions. Traditional power converters, such as simple DC/DC converters or AC/DC systems, are limited in their ability to handle multiple power inputs and outputs simultaneously, which is a common requirement in modern renewable energy systems. Wind energy systems often require multiple output voltages to power various devices, such as energy storage systems, grid connections, and local loads. Moreover, wind conditions are highly variable, and the ability to track and extract the maximum power from the wind turbine is vital for optimizing the energy conversion process. Another key issue is the need for high-efficiency conversion. Conventional power converters tend to suffer from significant switching losses, especially at high power levels, which reduces the overall efficiency of the system. In renewable energy systems, where every bit of available energy is critical, maximizing efficiency is essential to ensure the system performs optimally and can meet the power demands of connected loads.

Multi-Input Multi-Output (MIMO) DC/DC Converters: To address these challenges, Multi-Input Multi-Output (MIMO) DC/DC converters have emerged as a promising solution. These converters are designed to simultaneously handle multiple input sources, such as wind turbines, solar panels, or energy storage systems, while providing multiple output voltages suitable for different applications. A MIMO converter offers several advantages over traditional single-input converters, including greater flexibility, increased power handling capability, and improved efficiency by integrating multiple renewable energy sources into a single power conversion system. A key feature of MIMO converters is their ability to manage different input sources, which is particularly important in hybrid renewable energy systems. For example, a wind power system may operate in conjunction with a solar power system, and a MIMO converter can efficiently combine the outputs from both sources while regulating the voltage levels to power different loads. This flexibility reduces the complexity of the system and improves its overall performance by consolidating power conversion into a single, highly efficient unit.

High-Efficiency Converter Design: The efficiency of power conversion is a fundamental aspect of any renewable energy system. High efficiency ensures that as much of the generated energy as possible is converted into usable power, minimizing losses that would otherwise waste valuable energy. The proposed MIMO DC/DC converter in this study focuses on optimizing efficiency through advanced techniques such as soft-switching, voltage clamping, and zero-voltage switching (ZVS). Soft-switching techniques are employed to reduce switching losses, which are a significant source of inefficiency in traditional power converters. By ensuring that the switch transitions occur when the voltage or current is zero, ZVS minimizes the energy lost during switching events. Voltage clamping further reduces switching stress and prevents damage to the converter, thereby increasing the converter's longevity and reliability. These techniques, when integrated into the converter design, contribute to substantial improvements in energy conversion efficiency. Another design feature that enhances efficiency is the use of a coupled inductor with a low turn ratio. This arrangement helps to achieve a high step-up voltage conversion, which is particularly important for wind energy systems that may require significant voltage boosts to meet the output requirements of connected loads. The coupled inductor also provides better energy transfer between the input and output stages, improving the overall power conversion process.

Maximum Power Point Tracking (MPPT) for Wind Energy Systems: To maximize the energy harvested from wind turbines, an essential technique used in renewable energy systems is Maximum Power Point Tracking (MPPT). MPPT algorithms continuously monitor the operating conditions of the wind turbine, such as wind speed and rotor speed, and adjust the operating point to extract the maximum possible power from the turbine. Wind turbines have a specific operating point—referred to as the maximum power point—at which they produce the highest amount of power for a given wind speed. Tracking and maintaining this operating point is critical for optimizing energy production and ensuring that the system operates at peak efficiency. MPPT algorithms are typically implemented in the control systems of wind turbines to dynamically adjust the power output. The proposed MIMO DC/DC converter integrates an MPPT algorithm that works in conjunction with the wind turbine to continuously adapt to changing wind conditions. By adjusting the converter's operating parameters in real-time, the MPPT algorithm ensures that the maximum amount of power is extracted from the wind turbine, improving the overall efficiency of the wind energy system.

Soft-Switching Techniques for Improved Efficiency: Switching losses in power converters can significantly reduce efficiency, especially in high-power applications such as wind energy systems. Soft-switching techniques, which include voltage clamping and zero-voltage switching (ZVS), are employed to mitigate these losses. ZVS ensures that switches in the converter operate when the voltage across them is zero, reducing the energy dissipated during switching events. This results in less heat generation and more efficient power

conversion. Additionally, voltage clamping helps prevent excessive voltage spikes that can occur during the switching process, thereby protecting the components from damage and improving the overall reliability of the converter. By combining these techniques, the proposed MIMO DC/DC converter minimizes switching losses and improves energy conversion efficiency.

Auxiliary Inductor and Energy Management: In renewable energy systems, managing the energy distribution across multiple outputs is a key consideration. The proposed MIMO DC/DC converter employs an auxiliary inductor to regulate the voltage of the auxiliary output. This feature ensures that the system can effectively manage energy flow to various loads, such as energy storage systems, the electrical grid, or other connected devices. By maintaining stable output voltages, the converter provides reliable power to diverse applications, even under fluctuating wind conditions. The auxiliary inductor also plays a role in optimizing the converter's performance by ensuring that energy is efficiently distributed across the outputs. This is particularly important in systems that require multiple voltage levels, such as microgrids or off-grid renewable energy systems. By employing an auxiliary inductor, the proposed converter can balance energy distribution and improve overall system performance.

Simulation Results and Validation: The proposed MIMO DC/DC converter has been extensively tested to validate its performance and efficiency. Experimental results demonstrate that the converter successfully operates under varying wind conditions and efficiently converts the energy harvested from wind turbines into stable output voltages for different loads. The results show that the converter achieves high efficiency and performance, making it suitable for use in wind power generation and other renewable energy systems that require multi-output configurations. The converter's ability to integrate MPPT control, soft-switching techniques, and auxiliary voltage regulation has been shown to significantly improve the overall efficiency of the system, reducing power losses and enhancing the stability of the output. These results validate the potential of the proposed converter in providing an efficient and reliable solution for renewable energy systems, particularly those that rely on wind power.

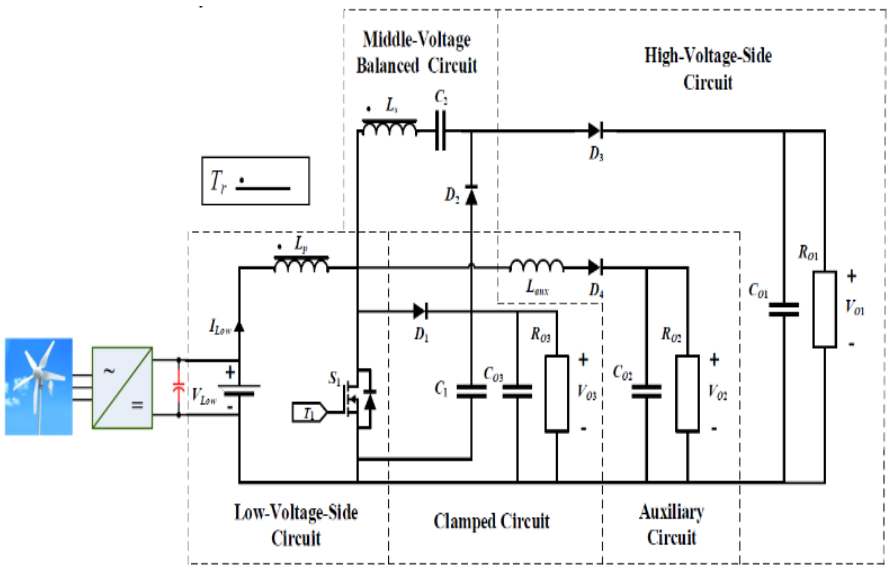

FIGURE 1. Proposed Block diagram of the of high-efficiency Multi-input triple-outputs dc/dc converter

Operation Principle and Steady-State Analyses: The system configuration for the proposed high-efficiency single-input triple-outputs dc/dc converter (HMTDC) topology is depicted in Fig. 1. The major symbol representations are expressed as follows. In Fig. 1, the low-voltage-side circuit (LVSC) is composed of the low-voltage switch (1 S), the primary-side winding (p L) of the coupled inductor (r T), and the low-voltage input terminal (Low V). By turning the low-voltage switch (1 S) on/off to draw/release energy to the secondary-side winding (s L) of the coupled inductor (r T). Then, the clamped circuit is composed of the clamped diode (D1), the clamped capacitor (C1), the middle-voltage filter capacitor (CO3), and the middle-voltage output terminal (O 3 V). It mainly absorbs the energy stored in the primary-side leakage inductor (k L) for protecting the low-voltage switch (1 S) and releasing energy to the middle-voltage capacitor (C2) and the middle-voltage output terminal (O 3 V). Moreover, the middle-voltage balanced circuit has the middle-voltage capacitor (C2), the middle-voltage balanced diode (D2), and the secondary-side winding (s L) of the coupled

inductor (r T). It mainly absorbs energy stored in the clamped capacitor (C1) and the middle-voltage filter capacitor (CO3) for boosting the voltage conversion ratios and releasing energy to the high-voltage dc bus terminal (O1 V). In addition, the high-voltage-side circuit (HVSC) has the high-voltage diode (D3), the high-voltage filter capacitor (CO1), and the high-voltage dc bus terminal (O1 V). It mainly releases energy to the high-voltage dc bus terminal (O1 V) through the high-voltage diode (D3). Furthermore, the auxiliary circuit contains the auxiliary inductor (aux L), the auxiliary diode (D4), the auxiliary source filter capacitor (CO 2), and the auxiliary source output terminal (O 2 V). It can charge the auxiliary source for peripheral components usage. Low V (Low I) denotes the voltage (current) of the input power source at the LVSC. O1 R, O2 R , and O3 R express the equivalent loads for the high-voltage dc bus terminal (O1 V), the auxiliary source output terminal (O 2 V), and the middle-voltage output terminal (O 3 V), respectively. 1 T is the driving signal for the low-voltage switch (1 S). The proposed HMTDC has three output ports with different voltage levels, and only one low-voltage input port. In this study, the output terminals are defined as the high-voltage dc bus (O1 V), the auxiliary source (O 2 V), and the middle-voltage output terminal (O 3 V), respectively. In order to simplify the description for the output powers of the proposed HMTDC, individual output powers can be denoted as 2 111 = / OO O P V R for the high-voltage dc bus terminal, 2 222 = / OO O P V R for the auxiliary source terminal, and 2 333 = / OO O P V R for the middle-voltage output terminal, respectively. Moreover, the total output power can be expressed as 123 T + + = OO O O P PP P. The proposed HMTDC has two essential characteristics for boosting input voltage and generating different voltage levels. To simplify the mathematic derivations, all of the voltages across a power switch and diodes are ignored. Moreover, it is assumed that the clamped capacitor (C1) and the middle-voltage capacitor (C2) are large enough to be considered as constant voltage sources C1 V and C 2 V , respectively.

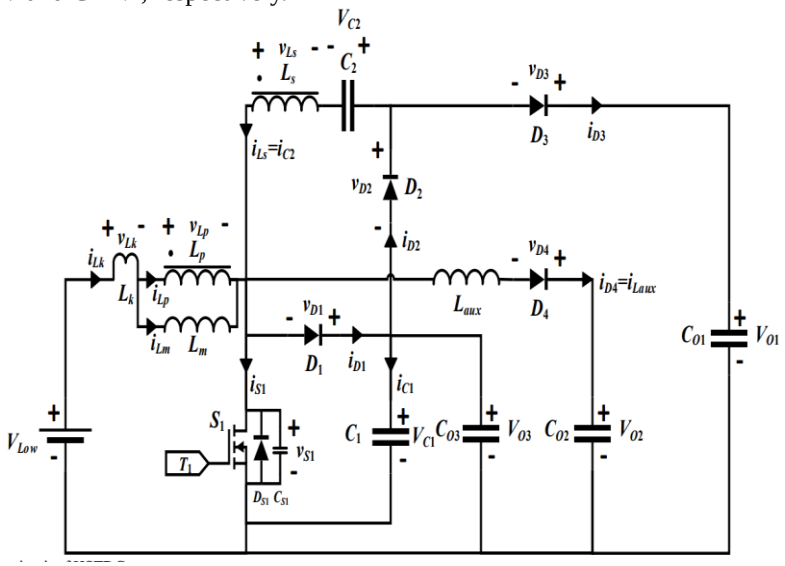

FIGURE 2. Equivalent circuit of HMTDC

Figure 2 shows the equivalent circuit of the proposed HMTDC, and the operation of the proposed HMTDC is explained as follows. The equivalent circuit of the coupled inductor (r T) are composed of the primary-side winding (p L), the secondary-side winding (s L), the primary-side magnetizing inductor (m L), and the primary-side leakage inductor (k L). By defining the turns ratio (N) to be equal / N N s p and labelling the voltage of Lp v and Ls v across the windings p L and s L , the turns ratio (N) can be represented as

$$v_{Ls} / v_{Lp} = N$$

Moreover, the coupling coefficient of the coupled inductor (r T) can be expressed as

$$k = L_m / (L_k + L_m)$$

In Fig. 2, CS 1 and DS1 are the intrinsic capacitance and the body diode of the power switch. In order to simplify theoretical analyses, the power switch and diodes in the proposed converter are considered as ideal components. The switch (1 S) is served as the main switch and is controlled for regulating the voltages of the

HVSC and the middle-voltage output terminal. Moreover, the diodes (D1, D2, D3, and D4) are conducted when the voltages of anodes are higher than the voltages of cathodes. The diodes (D2 and D3) are conducted complementarily when the switch (1 S) is turned on/off. The duty cycle of the power switch (1 S) is defined as 1 d, and one switching cycle is denoted as S T. Due to the coupled inductor with a good coupling effect, the leakage energy is much smaller than the energy of a ferrites powder core. Because the proposed circuit topology has excellent voltage clamping property, the leakage energy can be fully absorbed. For simplifying mathematical derivations, the coupling coefficient is assumed to be k = 1.

The voltage gain (GV1) of the proposed HMTDC from the LVSC to the HVSC can be represented as

$$G_{V1} = \frac{V_{O1}}{V_{Low}} = \frac{N+2}{1-d_1}$$

Moreover, the voltage gain (GV 3) of the proposed HMTDC from the LVSC to the middle-voltage output terminal (O 3 V) can be calculated as

$$G_{V3} = \frac{V_{O3}}{V_{Low}} = \frac{1}{1-d_1}$$

In addition, the voltage gain (GV 2) of the proposed HMTDC from the LVSC to the auxiliary source (O 2 V) can be expressed as

$$G_{V2} = \frac{V_{O2}}{V_{Low}} = \frac{2}{(1-d_1)+\sqrt{(1-d_1)^2+[8L_{aux}/(R_{O2}T_S)]}}$$

Mathematical Modeling of Seig-Based Wind Farm

The SEIG wind turbine makes use of the wound rotor induction generator shown in Figure 2 in conjunction with a wind turbine. The rotor is powered by two IGBT bridge–voltage source converters connected to a DC link in this generator's two-way power converter. Variations in turbine speed are possible thanks to the power converter's ability to dynamically modify grid and rotor frequencies. In the event of strong winds, the turbine rotor's blade angle can be adjusted to limit the power and rotational speed.

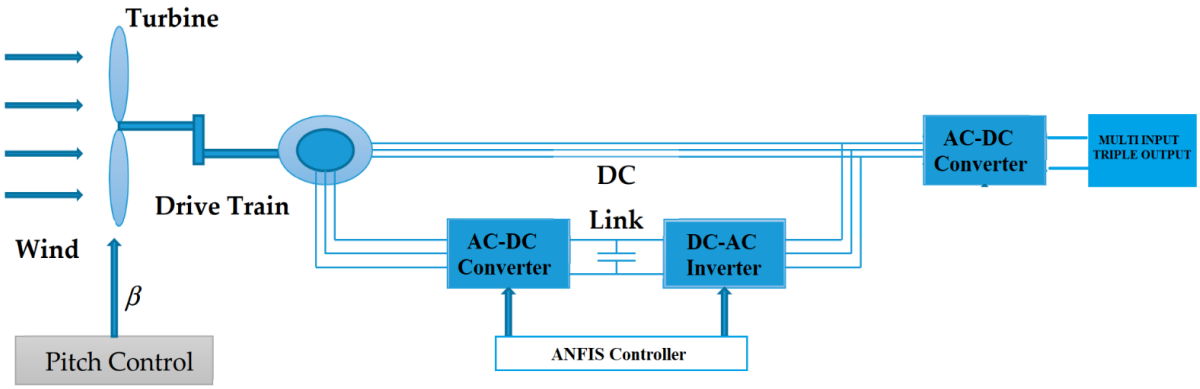

FIGURE 3. Wind Turbine and SEIG Modelling

Wind turbine (WT) mechanical power generation is given as:

$$P_m = \frac{1}{2}\rho A c_p(\lambda,\beta) v_{wind}^3 \quad (1)$$

Cp is the performance coefficient, which is defined a

$$c_p = \frac{P_m}{P_{wind}} \tag{2}$$

The Tip Speed Ratio (TSR) is

$$\lambda = \frac{\omega_r}{v_{wind}} \tag{3}$$

The performance coefficient is expressed as

$$c_p(\lambda,\beta) = c_1\left(\frac{c_2}{\lambda_x} - c_3\beta - c_4\right)e^{-\left(\frac{c_5}{\lambda_i}\right)} + c_6\lambda \tag{4}$$

$$\frac{1}{\lambda_x} = \frac{1}{\lambda + 0.08\beta} - \frac{0.035}{\beta^3 + 1} \tag{5}$$

where ρ = density of air, A = impact area of the blade, v wind = expected wind speed, ωr = synchronous speed, and β = blade pitch angle. The drop-in, estimated, and pull-out wind speeds of the WT are 4, 14, and 24 m/s respectively. The wind turbine's two-inertia decreased-order comparable mass-spring-damper configuration combined with the wind SEIG's rotor shaft is used with an identical gearbox. The equations of motion per unit (pu) can be applied to ref. [14]. The windings designed for the SEIG stator are conveniently attached to a 0.69/33 kV step-up transformer's low-voltage section, whereas the windings on the rotor side SEIG are linked to the same side by a SEIG side Converter, DC link, and Grid Side inverter (GSI). The SEIG circuit diagram is the same as that of the system of induction generator [15]. The SEIG model can be done as follows:

$$\frac{X'_s di_{ds}}{\omega_s dr} = v_{ds} - \left[R_s + \frac{1}{\omega_s T'_o}(X_s - X'_s)\right] \times i_{ds} - (1 - s_r)E'_d - \frac{L_m}{L_{rr}}v_{dr} + \frac{1}{\omega_s T'_o}E'_q + X'_s i_{qs} \tag{6}$$

$$\frac{X'_s di_{qs}}{\omega_s dt} = v_{qs} - \left[R_s + \frac{1}{\omega_s T'_o}(X_s - X'_s)\right] \times i_{qs} - (1 - s_r)E'_q - \frac{L_m}{L_{rr}}v_{qr} - \frac{1}{\omega_s T'_o}E'_d - X'_s i_{ds} \tag{7}$$

$$\frac{dE'_d}{dt} = -s_r\omega_s E'_d + \omega_s\frac{L_m}{L_{rr}}v_{dr} - \frac{1}{T'_o} \times \left[E'_d + (X_s - X'_s)i_{qs}\right] \tag{8}$$

$$\frac{dE'_q}{dt} = -s_r\omega_s E'_d + \omega_s\frac{L_m}{L_{rr}}v_{dr} - \frac{1}{T'_o} \times \left[E'_q - (X_s - X'_s)i_{ds}\right] \tag{9}$$

The DC link equation can be given as follows

$$Cv_{DC}\frac{dv_{DC}}{dt} = v_{dg}i_{dg} + v_{qg}i_{qg} - \left(v_{dr}i_{dr} + v_{qr}i_{qr}\right) \tag{10}$$

where Lss and Lrr are the self-inductance of the stator and rotor side respectively; Lm is the mutual inductance; Rs is the resistance of the rotor side; T 0 o is the time constant of the rotor circuit; ωs is the synchronous angle speed; sr is the rotor slip; Xs is the stator reactance; X 0 s is the transient reactance of the stator side; E 0 d and E 0 q are the voltage behind the transient reactance d-axis and q-axis respectively; ids represent the d-axis stator currents; iqs represents the q-axis stator currents; Vds and Vqs represent the stator voltages of the d and q side, respectively; Vdr and Vqr are the rotor voltages of the d and q side, respectively. VDC is the DC link voltage; idr and iqr are the rotor side d and q-axis currents, respectively; idg and iqg are the grid side d and q-axis currents; Vdg and Vqg are the grid side d and q-axis voltages, respectively; and iDC is the condenser current.

The rotor section of the converter regulates the power output and monitors the adjustment of the terminal voltage. The diagrams for the control block are seen in Figure 3a. The equations for control are given by [15]:

$$\frac{dx_2}{dt} = i_{qr\_ref} - i_{qr} = K_{p1}\left(P_{ref} + P_s\right) + K_{i1}x_1 - i_{qr} \text{ and } \frac{dx_3}{dt} = v_{s_{ref}} - v_s \quad (12)$$

$$i_{dr\_ref} = K_{p3}\left(v_{s_{ref}} - v_s\right) + K_{i3}x_3 \quad (13)$$

$$\frac{dx_4}{dt} = i_{dr\_ref} - i_{dr} = K_{p3}\left(v_{s_{ref}} - v_s\right) + K_{i3}x_3 - i_{dr} \quad (14)$$

$$v_{qr} = K_{p2}\left(K_{p1}\Delta P + K_{i1}x_1 - i_{qr}\right) + K_{i2}x_2 + s_r\omega_s L_m i_{ds} + s_r\omega_s L_{rr} i_{qr} \quad (15)$$

$$v_{dr} = K_{p2}\left(K_{p3}\Delta v + K_{i3}x_3 - i_{dr}\right) + K_{i2}x_4 - s_r\omega_s L_m i_{qs} - s_r\omega_s L_{rr} i_{dr} \quad (16)$$

where kp1 is the proportional power regulator gain; ki1 is the integrating power regulator gain; kp2 is the proportional gain of rotor side; ki2 is the integrating rotor side converter gain; kp3 is the proportional GSI gain; Ki3 is the integrating GSC gain; idr_re f represents the d-axis current control component of the GSI, and iqr_re f represents the q-axis current control part of the turbine side operator

Dynamic Model of Seig-Based Wind Turbine

The dynamic model of the SEIG-based wind turbine can be compactly written using above Equations (14)–(20) as

$$\dot{x} = f(x, y, z) \quad (17)$$

$$z = g(x, u) \quad (18)$$

where x = state variables of SEIG, z = output variables, and u = input variables. From all the above-given equations, the SEIG model can be written as,

$$z = \left[v_{dr}, v_{qr}, v_{dg}, v_{qg}\right]^T \quad u = \left[v_{ds}, v_{qs}, v_{dg}, v_{qg}\right]^T \quad (19)$$

$$x = \left[\omega, \beta, \tilde{\theta}_{tw}, s, i_{ds}, i_{qs}, E'_d, E'_q, x_1, x_2, x_3, x_4, v_{DC}, x_5, x_6, x_7\right]^T. \quad (20)$$

Voltage Control Via Switching Capacitor Bank Technique

Switching:
As a result of the transitory voltage and current transients that can occur, capacitor switching has been ruled out in the past. Current "spikes," for example, have been argued to be justified in exceeding the maximum current rating and the (di/dt) value of a specific semiconductor switch. Designing a semiconductor switch to survive the transient value at the switching instant is the only way out of this conundrum! This condition with the switching capacitor bank is explained by the analogous circuit in Fig. 2, which shows how it came about due to the duty cycle. Detailed information on this circuit may be found in Ref. [6]. Fig. 2's switches are operated in anti-phase, meaning that the fs2 which controls switch S2 is the inverse function of fs1 which controls switch S1. When switch S1 is open, switch S2 is closed; when switch S1 is closed, switch S2 is open.

Voltage Control:
This is shown in figure 1. The voltage error is sent to the controller, which then sends out a duty cycle. The value of is used as an input to the semiconductor switches so that the value of the capacitor bank can be changed to meet the needs of the effective value of the excitation, which is what the switches do. It is done this way because automatic switching of the capacitor bank makes it possible to change the self-excitation and control the terminal voltage.

Frequency Control:
To regulate the system's frequency, the pitch angle of the turbine blades is changed to a different value. Using this, the SEIG can maintain a consistent stator frequency while also mitigating the effects of speed disturbances. The wind turbine's WECS power coefficient (Cp) determines the pitch angle. Based on Equation (12) in Appendix C, the pitch angle value is used to determine (Cp). As a result, optimizing the pitch angle value leads to better mechanical power control and, ultimately, better system frequency adaption. Accordingly, the wind turbine's mechanical power is controlled by frequency control.

2. SIMULATION RESULTS

In order to verify the effectiveness of the proposed high-efficiency Multi-input triple-outputs dc/dc converter (HMTDC) in practical applications, the experimentations of the proposed HMTDC are provided in this section. According to the circuit analyses in Section II, the circuit components and the electrical specifications of the proposed HMTDC are summarized in Tables I and II, respectively. For the stable operation of the proposed HMTDC, the feedback control is used to solve the problem of the output voltage varied with load variations. In this control scheme, a conventional proportional-integral (PI) controller without complex mathematical dynamic models is utilized. In this study, the output voltages (i.e., the high-voltage dc bus (O1 V) and the middle-voltage output terminal (O 3 V)) of the proposed HMTDC are controllable via the conventional PI control framework, and the voltage level of the auxiliary source (O 2 V) is regulated by the design of the auxiliary inductor (aux L). Although the voltage of the auxiliary source (O 2 V) is incontrollable real time, the predetermined voltage range by the design of the auxiliary inductor (aux L) is appropriate to provide the floating charge voltage for an energy storage device (e.g., a battery module) as the load in the auxiliary circuit.
The measured waveforms of the power switch (1 S), diodes (D1 , D2 , D3 and D4), and the coupled inductor (r T) of the proposed HMTDC under the total output power T P = O 500W (1 PO = 330W , 2 PO = 70W , and 3 PO = 100W) are depicted in Fig. 3, where the input voltage at low-voltage-side circuit (LVSC) is considered as V = Low 12V . From Fig. 3(a), the leakage inductor restricts the instantaneous current change, and the current direction could not be changed immediately in the auxiliary inductor. It is obvious that power switch (1 S) is turned on under the property of zero-current switching (ZCS) so that the corresponding switching loss can be reduced. Moreover, the voltage across the power switch (1 S) is clamped at 40V. As can be seen from Fig. 3(b), when the power switch (1 S) is turned off, the clamped diode (D1) is conducted to transfer the energy stored in the leakage inductor to the clamped capacitor (C1), and the reverse-recovery current inside the clamped diode (D1) is approximately zero due to the selection of a schottky diode. From Fig. 3(c), the middle-voltage balanced diode (D2) is conducted to transfer the energy to the middle-voltage capacitor (C2) from the secondary-side winding (s L), the clamped capacitor (C1), and the middle-voltage filter capacitor (CO3). Due to the selection of a schottky diode, the reverse-recovery current inside the middle-voltage balanced diode (D2) is also approximately zero. As can be seen from Fig. 3(d)-3(e), the high-voltage diode (D3) and the auxiliary diode (D4) are conducted when the diodes are forward bias, and the energy is delivered to the high-voltage dc bus (O1 V) and the auxiliary source (O 2 V), respectively. Because there is no reverse-recovery current inside the high-voltage diode (D3) and the auxiliary diode (D4), the effect of the electromagnetic interference (EMI) can be alleviated, and the power consumption on the diodes can be decreased for the high power conversion. In addition, the current waveforms of the primary-side magnetizing inductor (Lmi), the primary-side winding (Lpi), and the secondary-side winding (Ls i) inside the coupled inductor (Tr) are depicted in Fig. 3(f). It is obvious that the proposed HMTDC is operated at CCM owing to the minimum value of Lmi to be larger than zero. The corresponding waveforms of the input voltage (Low V) and three output voltages (O1 V , O 2 V and O 3 V) are depicted in Fig. 4. From Fig. 4, the output voltages can be stably controlled to achieve the desired values via the feedback control.

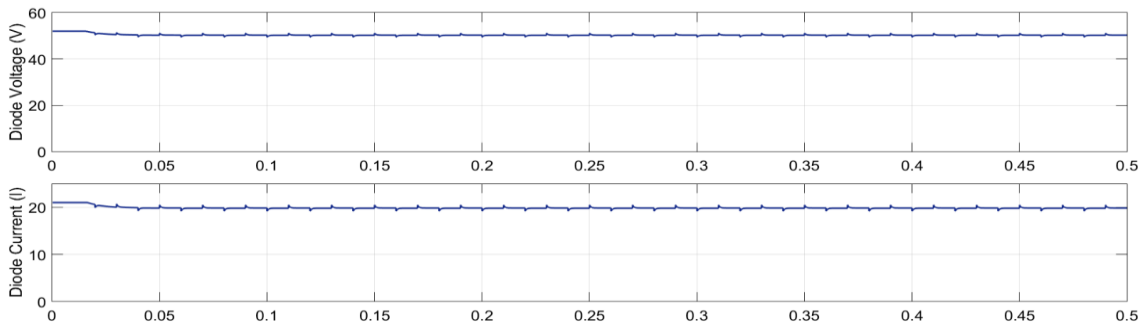

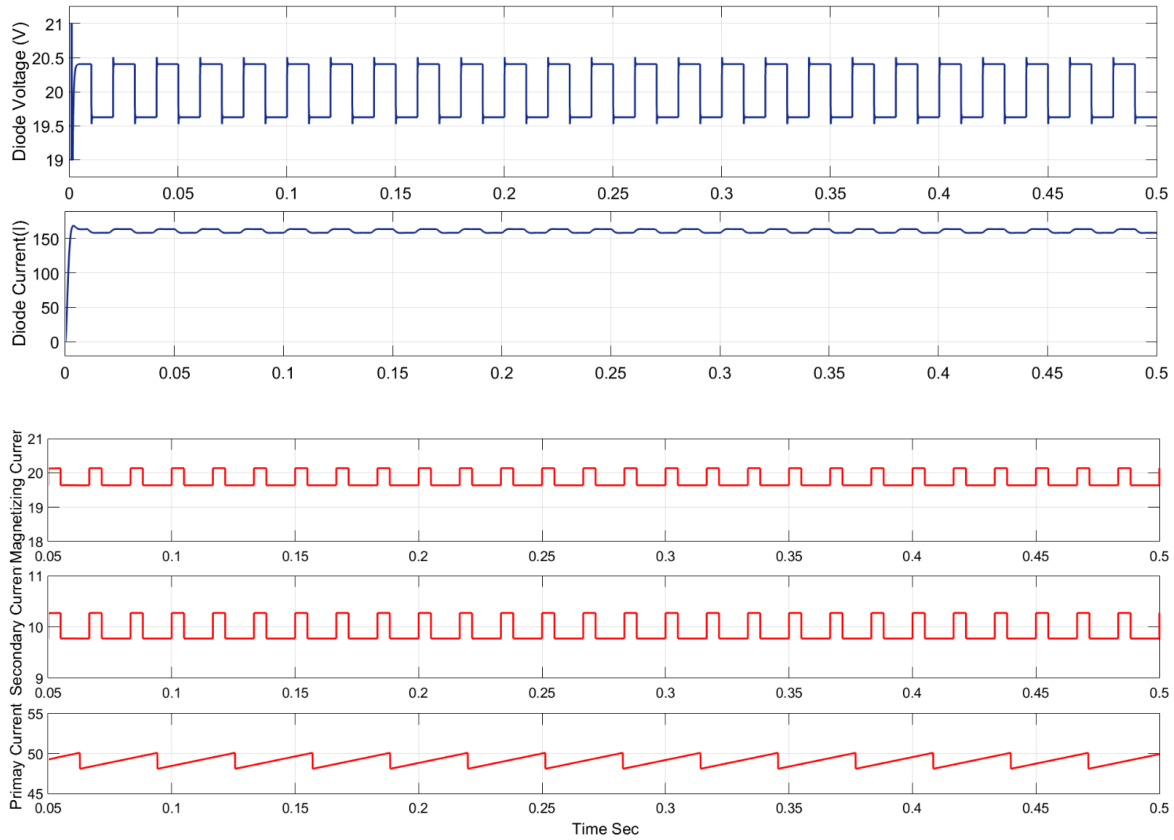

FIGURE 4. Simulation waveforms of switch, diodes, and coupled inductor at POT=500W: (a) S1; (b) D1; (c) D2; (d) D3; (e) D4; (f) Tr

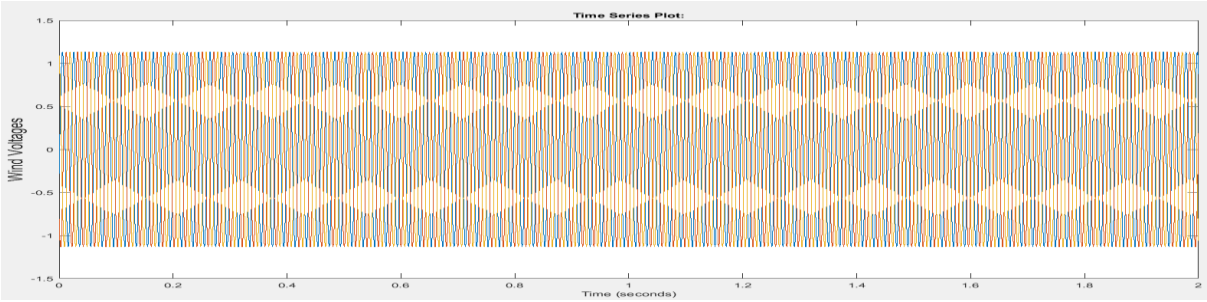

(a)

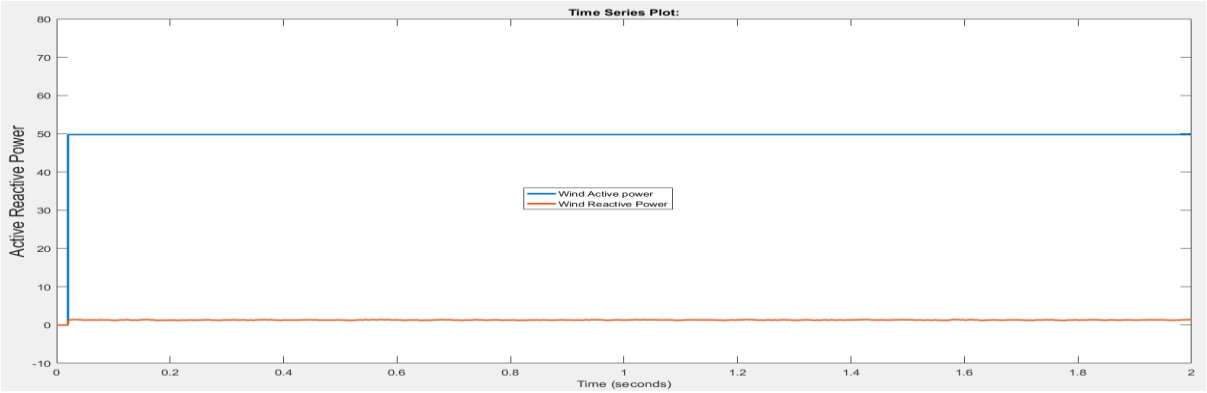

(b)

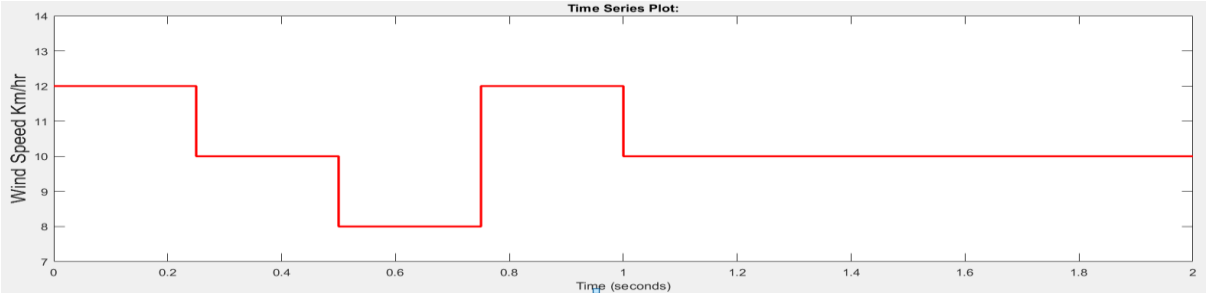

(c)

FIGURE 5. (a) Voltages (b) active power (c) Wind speed

Fig 5. Dynamic Response on Variation of wind speed Shows the Voltages, Reactive power, active power, and Wind speed of SEIG at time t=1 a small disturbance occurs in the active power and reactive power due to the loads.

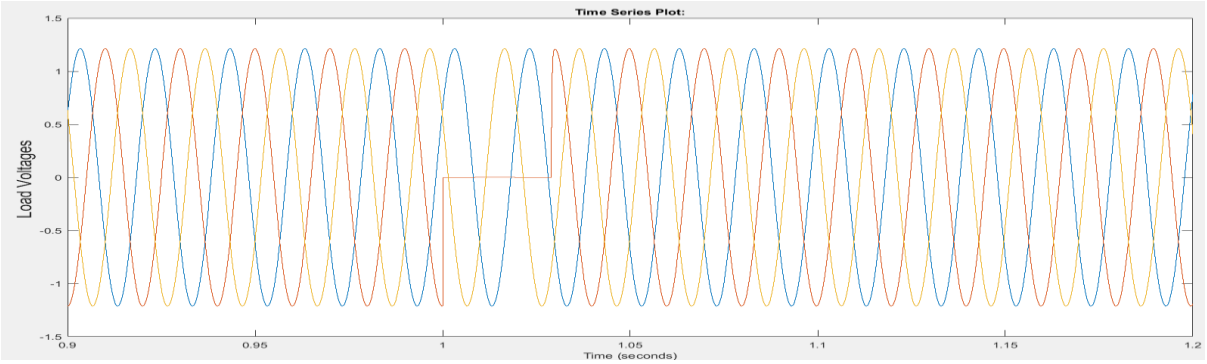

(a)

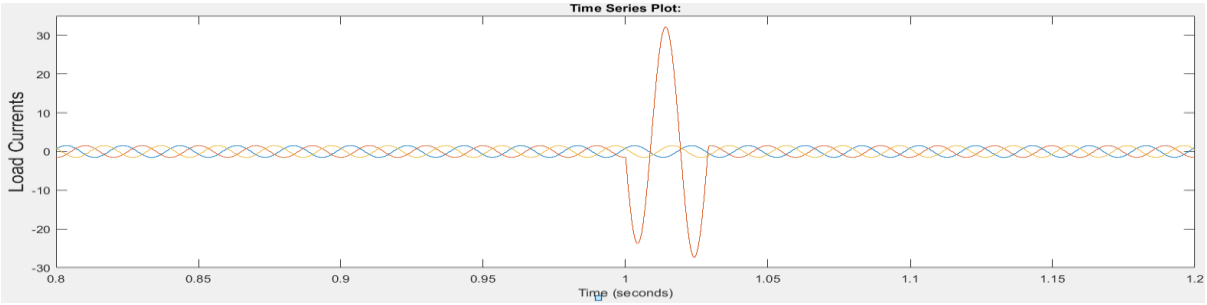

(b)

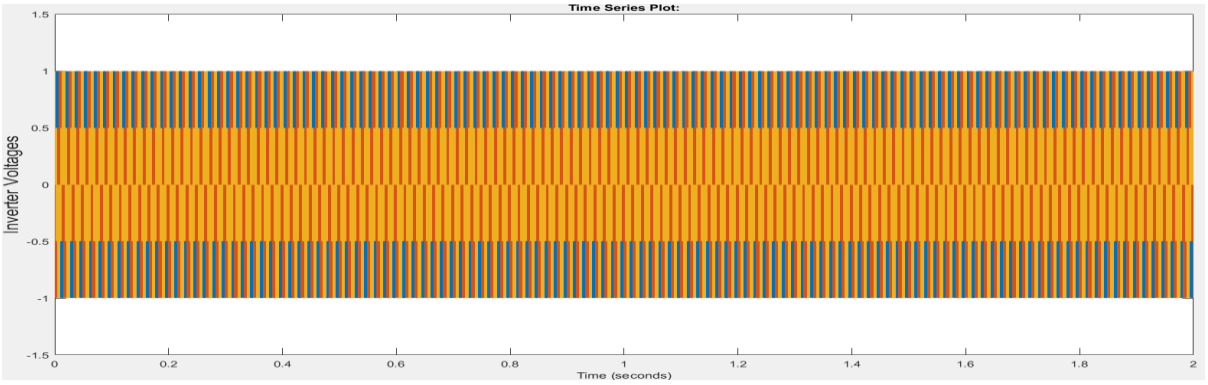

(c)

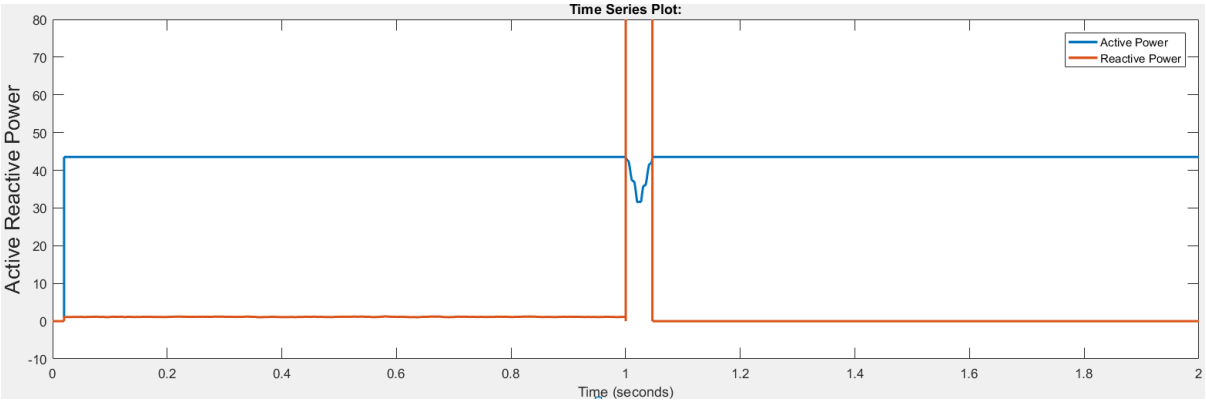

(d)

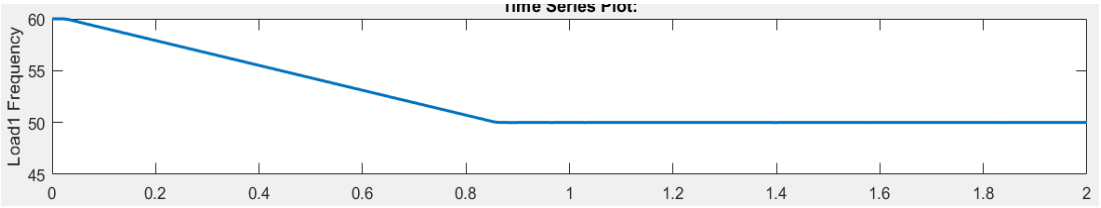

(e)

FIGURE 6. (a) Voltages (b) currents (c) active power (d) Reactive power (e) Inverter Voltage (f) frequency of the linear load

Fig 6. Dynamic Response on Variation of Linear Load Shows the Voltages, active power, Reactive power, and frequency of the linear load at time t=1 a small disturbance occurs in the active power and reactive power due to the loads, and in the fig7(f) frequency is dropped from 60Hz to 50Hz at the time period of 0.9sec. and it was maintained at 50Hz.

The transient responses of the proposed HMTDC under step output-power changes between T P = O 500W and T P = O 1kW are depicted in Fig. 5. Although there are little voltage variations under step output-power changes, the voltage levels for the high-voltage dc bus terminal, the middle-voltage output terminal, and the auxiliary source terminal can be stably adjusted. Moreover, the output voltage responses of the proposed HMTDC under the corresponding nominal input voltage 12V to be varied ±10% are depicted in Fig. 6. Although there are little voltage variations under input voltage change from 12V to 13.2V, three output voltages (O1 V , O 2 V and O 3 V) can be stably adjusted at desired values. As for input voltage change from 13.2V to 10.8V, three output voltages (O1 V , O 2 V and O 3 V) also can be stably adjusted at desired values. Although the output voltage of the auxiliary circuit only can be adjusted at the setting range 25V~30V via the design of the auxiliary inductor, the output voltages of the high-voltage dc bus and the middle-voltage output terminal can be precisely controlled to be 200V and 40V, respectively. The waveforms including the power conversion efficiency and three output powers of the proposed HMTDC are depicted in Fig. 7(a).

3. CONCLUSION

This study presented the development of a high-efficiency multi-input multi-output (MIMO) DC/DC converter integrated with wind energy and a wind maximum power point tracking (MPPT) algorithm, specifically designed for renewable energy applications. The proposed MIMO converter effectively addresses the need for multiple output voltages in wind-powered systems, ensuring stable and efficient power delivery to diverse loads. By utilizing a coupled inductor with a low turn ratio, the converter achieves significant voltage gain, while the MPPT algorithm optimizes power extraction from the wind turbine under varying environmental conditions. The implementation of soft-switching techniques, including voltage clamping and zero-voltage switching (ZVS), further enhances system efficiency by minimizing switching losses. Additionally, the use of an auxiliary inductor for regulating auxiliary output voltages enables effective energy management across multiple outputs, ensuring robust and reliable performance. Experimental results confirmed the high efficiency and effectiveness of the proposed converter, demonstrating its suitability for wind power generation systems and other renewable energy applications requiring multi-output configurations. In conclusion, the developed

MIMO DC/DC converter provides a promising solution for improving energy conversion efficiency and optimizing power management in renewable energy systems, particularly those utilizing wind power. Future work can focus on further optimization of the control strategies and the integration of additional renewable energy sources to broaden the application scope of this converter in diverse energy systems.

REFERENCES

[1]. T. Laura, V. I. Enric, M. A. Javier, M. P. Sylvia, and M. S. Luis, "Seamless sliding-mode control for bidirectional boost converter with output filter for electric vehicles applications," IET Power Electron., vol. 8, no. 9, pp. 1808-1816, Sep. 2015.

[2]. R. T. Naayagi, A. J. Forsyth, and R. Shuttleworth, "Performance analysis of extended phase-shift control of DAB dc-dc converter for aerospace energy storage system," IEEE Conf. Power Electron and Drive Systems., pp. 514-517, Jun. 2015.

[3]. J. M. Shen, H. L. Jou, and J. C. Wu, "Transformerless single-phase three-wire line-interactive uninterruptible power supply," IET Power Electron., vol. 5, no. 9, pp. 1847-1855, Nov. 2012.

[4]. Z. Amjadi and S. S. Williamson, "Prototype design and controller implementation for a battery-ultracapacitor hybrid electric vehicle energy storage system," IEEE Trans. Smart Grid, vol. 3, no. 1, pp. 332-340, Mar. 2012

[5]. J. Cao and A. Emadi, "A new battery/ultracapacitor hybrid energy storage system for electric, hybrid, and plug-in hybrid electric vehicles," IEEE Trans. Power Electron., vol. 27, no. 1, pp. 122-132, Jan. 2012.

[6]. X. H. Liu, H. Li, and Z. Wang, "A fuel cell power conditioning system with low-frequency ripple-free input current using a control-oriented power pulsation decoupling strategy," IEEE Trans. Power Electron., vol. 29, no. 1, pp. 159-169, Jan. 2014.

A. Urtasun, P. Sanchis, and L. Marroyo, "Adaptive voltage control of the dc/dc boost stage in PV converters with small input capacitor," IEEE Trans. Power Electron., vol. 28, no. 11, pp. 5038-5048, Nov. 2013.

[7]. J. Yao, H. Li, Z. Chen, X. F. Xia, X. Y. Chen, Q. Li, and Y. Liao, "Enhanced control of a DFIG-based wind-power generation system with series grid-side converter under unbalanced grid voltage conditions," IEEE Trans. Power Electron., vol. 28, no. 7, pp. 3167-3181, Jul. 2013.

A. Nahavandi, M. T. Hagh, and M. B. Bannae, "A nonisolatedmultiinput multioutput dc-dc boost converter for electric vehicle applications," IEEE Trans. Power Electron., vol. 30, no. 4, pp. 1818-1835, Apr. 2015.

[8]. M. Forouzesh, Y. Shen, K. Yari, Y. P. Siwakoti, and F. Blaabjerg, "High-efficiency high step-up dc-dc converter with dual coupled inductors for grid-connected photovoltaic systems," IEEE Trans. Power Electron., vol. 33, no. 7, pp.5967-5982, Jul. 2018.

[9]. Y. P. Siwakoti and F. Blaabjerg, "Single switch nonisolated ultra-step-up dc-dc converter with an integrated coupled inductor for high boost applications,'' IEEE Trans. Power Electron., vol. 32, no. 11, pp. 8544-8558, Nov. 2017.

